Macromolecules

Article

Study on the Origin of Inverted Phase in Drying Solution-Cast Block Copolymer Films

Haiying Huang, Fajun Zhang, Zhijun Hu, Binyang Du, and
Tianbai HeFuk Kay Lee, Yongjian Wang, and Ophelia K. C. Tsui

More About This Article

Additional resources and features associated with this article are available within the HTML version:

- Supporting Information
- Links to the 9 articles that cite this article, as of the time of this article download
- Access to high resolution figures
- Links to articles and content related to this article
- Copyright permission to reproduce figures and/or text from this article

View the Full Text HTML

ACS Publications
High quality. High impact.

Study on the Origin of Inverted Phase in Drying Solution-Cast Block Copolymer Films

Haiying Huang, Fajun Zhang, Zhijun Hu, Binyang Du, and Tianbai He*

State Key Laboratory of Polymer Physics and Chemistry, Changchun Institute of Applied Chemistry, Chinese Academy of Sciences, Changchun, 130022, P. R. China

Fuk Kay Lee, Yongjian Wang, and Ophelia K. C. Tsui*

Physics Department, Hong Kong University of Science and Technology, Clear Water Bay, Hong Kong, P. R. China

Received December 13, 2002

ABSTRACT: In a previous study, we reported observation of the novel inverted phase (the minority blocks comprising the continuum phase) in kinetically controlled phase separating solution-cast poly(styrene-*b*-butadiene-*b*-styrene) (SBS) triblock copolymer films [Zhang et al. *Macromolecules* **2000**, *33*, 9561−7]. In this study, we adopt the same approach to investigate the formation of inverted phase in a series of solution-cast poly(styrene-*b*-butadiene) (SB) asymmetric diblock copolymers having nearly equal polystyrene (PS) weight fraction (about 30 wt %) but different molecular weights. The microstructure of the solution-cast block copolymer films resulting from different solvent evaporation rates, R, was inspected, from which the kinetically frozen-in phase structures at qualitatively different block copolymer concentrations and correspondingly different effective interaction parameter, χ_{eff}, can be deduced. Our result shows that there is a threshold molecular weight or range of molecular weight below which the unusual inverted phase is accessible by controlling the solvent evaporation rate. In comparing the present result with that of our previous study on the SBS triblock copolymer, we find that the formation of the inverted phase has little bearing on the chain architecture. We performed numerical calculations for the free energy of block copolymer cylinders and found that the normal phase is always preferred irrespective of the interaction parameter and molecular weight, which suggests the formation of the inverted phase to have a kinetic origin. A mechanism based on kinetic effects is proposed to account for the observed threshold in molecular weight.

Introduction

Gaining control of the morphological transitions of block copolymers has aroused much research interest in recent years,[1–18] ascribable to the curiosity to understand the interesting sciences involved and the numerous applications perceivable by exploiting the material's microstructure. According to the mean-field theory for phase separation of diblock copolymer melt in the weak segregation limit,[19–22] the transitions between different kinds of morphologies are determined by the product, χN, where χ is the Flory−Huggins interaction parameter between the two blocks and N is the total degree of polymerization of the copolymer. It has been demonstrated that the different morphological phases can be reversibly attained by changing the temperature, T, by virtue of the relation, $\chi = A + B/T$ (where A and B are constants). Indeed, thermal means has thus far been the customary approach for inducing the order−order transition (OOT) and the order−disorder transition (ODT) of block copolymers. However, the range of χN hence afforded is often limited: Exceedingly low values of χN cause ODT to occur below the glass transition temperature of individual blocks, resulting in the kinetic suppression of the phase separation process; too high a value of χN makes the ODT occur at very high temperatures where the polymer is susceptible to thermal degradation. These problems are alleviated in block copolymers in solution. On one hand, the kinetics of microphase separation is improved; on the other hand,

the incompatibility between the two blocks is reduced. A large number of earlier studies had been devoted to the microphase separation of block copolymers in solution.[4−6,23−29] Microphase separation of block copolymers in good solvent is expected to take place in the semidilute regime in which the polymer chains interpenetrate extensively. In the theory of Fredrickson and Leibler, dedicated to deal with microphase separation in semidilute solutions,[21] the molten state theory was modified by incorporating both the excluded-volume and fluctuation effects. The product parameter, $\chi_{eff}Z$, was introduced (where χ_{eff} is the effective interaction parameter of the polymer solution and Z the number of "blobs" of size equal to the correlation length contained in a block copolymer chain) which replaces the role of χN in molten block copolymer in the phase diagram. Since $\chi_{eff}Z$ and χN are simply related, $\chi_{eff}Z \approx 0.67\chi N \varphi^{1.6}$ (where φ denotes the volume fraction of the polymer in the solution), the microphase of block copolymer solutions can be varied through changes in the polymer volume fraction, φ, besides the total degree of polymerization and temperature. Ideally, studies of such solvent-induced microphase separation should be carried out in nonvolatile solutions so as to ensure that φ is maintained constant with time. However, most polymer solvents are volatile; this requirement is difficult to realize in most block copolymer solutions. In a previous study,[29] we used different evaporation rates to kinetically freeze in different microstructures of cast films of poly(styrene-*b*-butadiene-*b*-styrene) (SBS) triblock (M_w = 140 kDa, PS wt % = 30%) 0.5 wt % in toluene. The faster the solvent evaporation rate is

* To whom correspondence should be addressed. E-mail phtsui@ust.hk (O.K.C.T.) or tbhe@ns.ciac.jl.cn (T.H.).

Table 1. Characterization of the Block Copolymers Used in This Work

specimen code	type of block copolymer	total $M_{n} \times 10^{-3}$ [a] (Da)	total $M_{w} \times 10^{-3}$ [b] (Da)	N[c]	PS (wt %)	PI[d]
SBS	S−B−S	116.67	140.00	1849	30	1.20
SB1	S−B	53.70	55.85	851	28.5	1.03
SB2	S−B	66.85[f]	73.93[f]	1059	30	1.11[f]
SB3	S−B	137.10[f]	137.30[f]	2210	27.2[e]	1.002
SB4	S−B	315.60	331.38	5000	28	1.05

[a] Number-average molecular weight. [b] Weight-average molecular weight. [c] Total degree of polymerization of block copolymer. [d] Polydispersity index. [e] Determined by ^{13}C NMR spectral analyses. [f] Determined from GPC data.

employed, the time scale allowed for the sample structure to evolve is shorter; therefore, microstructures (whether equilibrium or metastable) of lower polymer concentrations, and hence smaller χ_{eff}, are frozen in— presumably a particular equilibrium (or metastable) microstructure can be formed even in a kinetic process if the rate of that process is slow enough that majority of the chains can diffuse over a distance of its own size before the χ_{eff} parameter is changed to a value favoring a different microstructure. We uncovered an unconventional inverted phase, consisting of cylinders or spheres of PB (the major block) in a matrix of PS (the minor block) that was consistently formed when a fast evaporation rate was applied (corresponding to a drying time of ~20 min). Only under the slowest evaporation rate (approximately days per film) could the normal phase (i.e., PS cylinders in a matrix of PB) result. It has been suggested[29] that the inverted phase was either a kinetically frozen-in metastable state or an equilibrium microphase that could be envisaged only for very dilute solutions of a triblock in which χ_{eff} is small in the first place, and chain packing is more restrictive in the normal phase than in the inverted phase in the second place (as illustrated in Figure 6 of ref 29). Henceforth, the entropy gain in forming the inverted phase may overwhelm the energy cost of having a bigger SB interfacial area of the inverted phase.[29]

To substantiate these ideas, one should perform the same experiments, but with SB diblocks, and devise ways to adjust the relative size of the enthalpy effect to the effect of geometric entropy in the block copolymers. One way to achieve the latter is by varying the degree of polymerization, N, of the copolymer. Since the size of the microdomains (i.e., the cylinders or spheres), R, increases with N, the enthalpy increase associated with the larger SB contact of the inverted phase, being $\sim R^{2}$, must increase with N. On the other hand, the geometric entropy factor, being $\sim \ln(R/D)^{2}$, where D is the period of the microstructure, should be relatively insensitive to variations in N. In this paper, we report the result from a systematic study on the microstructure obtained from solution cast SB films of different molecular weights (but roughly the same PS wt %) at different evaporation rates. We uncovered that the inverted phase was formed in SB or SBS block copolymers with molecular weight less than a threshold molecular weight (or range of molecular weights), M_{w}^{*}, of 70−100 kDa, and at high evaporation rates. No effect could be detected from different chain architectures (i.e., diblock or triblock). By using the result of Helfand and Wasserman,[30] we calculated the mean-field free energy of microphase-separated diblock and triblock cylinders and found that the normal phase was always preferred at all molecular weights and interaction parameters of interest. The inverted phase is thus interpreted to be a metastable state formed at the transient when the chains just begin to overlap upon reaching the semi-

dilute regime, and phase separation starts to take place. The block that is more mobile can more quickly fill the space surrounding the more sluggish blocks, making the latter the cylindrical or spherical cores. When the total molecular weight is below ~100 kDa, the PS blocks are unentangled and hence will quite likely act as the more mobile block during the aforementioned transient.

Experimental Section

We summarize the detailed information about the block copolymers used in this study in Table 1, including one poly(styrene-*b*-butadiene-*b*-styrene) (SBS) triblock copolymer and four poly(styrene-*b*-butadiene) (SB1 to SB4) diblock copolymers of different molecular weights. The SBS and SB2 were purchased from Aldrich Chemical Co. Detailed information about the SBS sample can be found in our previous paper.[29] For SB2, we determined the molecular weight and polydispersity index by GPC (Waters 410 GPC) and the PS weight fraction by quantitative ^{13}C NMR spectral analyses (Unity 400 NMR, Varisan, Palo Alto, CA). The isomeric composition of the butadiene block characterized by ^{13}C NMR was found to contain 60.9% *trans*-1,4, 29.5% *cis*-1,4, and 9.6% vinyl isometric units. The SB1, SB3, and SB4 diblock copolymers were purchased from Polymer-source Inc. (Canada) and had come with detailed sample analyses by the manufacturer. As seen from Table 1, the SBS and SB block copolymers covered in this work have similar PS weight fractions of ~30%. Former studies show that these samples in the molten state should form hexagonally arranged PS cylinders in a continuum of PB.[19,31,32]

In the experiment, the block copolymers were dissolved in toluene, a good solvent of both PS and PB,[29] to produce 0.5 wt % solutions. We used a 20 μL pipet to cast equal-sized droplets of the solutions onto freshly cleaved mica. Then the films were dried at four different solvent evaporation rates at room temperature (~25 °C). The fastest evaporation rate ($Ra \approx 0.1$ mL/h) was achieved by placing the solution-cast films inside a cylindrical container of radius and height 2.5 and 3 cm, respectively, covered with a lid that contains 250 punched holes of about 0.6 mm diameter. The second fastest evaporation rate ($Rb \approx 1$ μL/h) was achieved by using a lid that has 50 punched holes instead. The third evaporation rate ($Rc \approx 0.2$ μL/h) was achieved by using a lid with no holes at all. To attain an even slower evaporation rate ($Rd \approx 0.05$ μL/h), the solution-cast film was exposed to toluene vapor of ~95% saturation for several days. To ensure that the comparison between microstructures of various samples (i.e., SBS and SB1 to SB4) from different solvent evaporation rates is reliable, at least one solution-cast film from each block copolymer was dried in parallel at any given evaporation rate.

The morphology of the samples developed after drying was examined by tapping-mode atomic force microscopy (TM-AFM) and transmission electron microscopy (TEM). TM-AFM measurements were carried out in a NanoScope IIIa scanning probe microscope (Digital Instruments Inc.) where phase contrast images of the sample surface were acquired. The PS and PB microdomains are clearly distinguishable in this imaging mode because of the very different viscoelasticities of the two polymers at room temperature. During imaging, the AFM cantilever (spring constant between 1.5 and 3.5 N m^{-1}) was driven to oscillate at ~400 kHz, close to the cantilever's
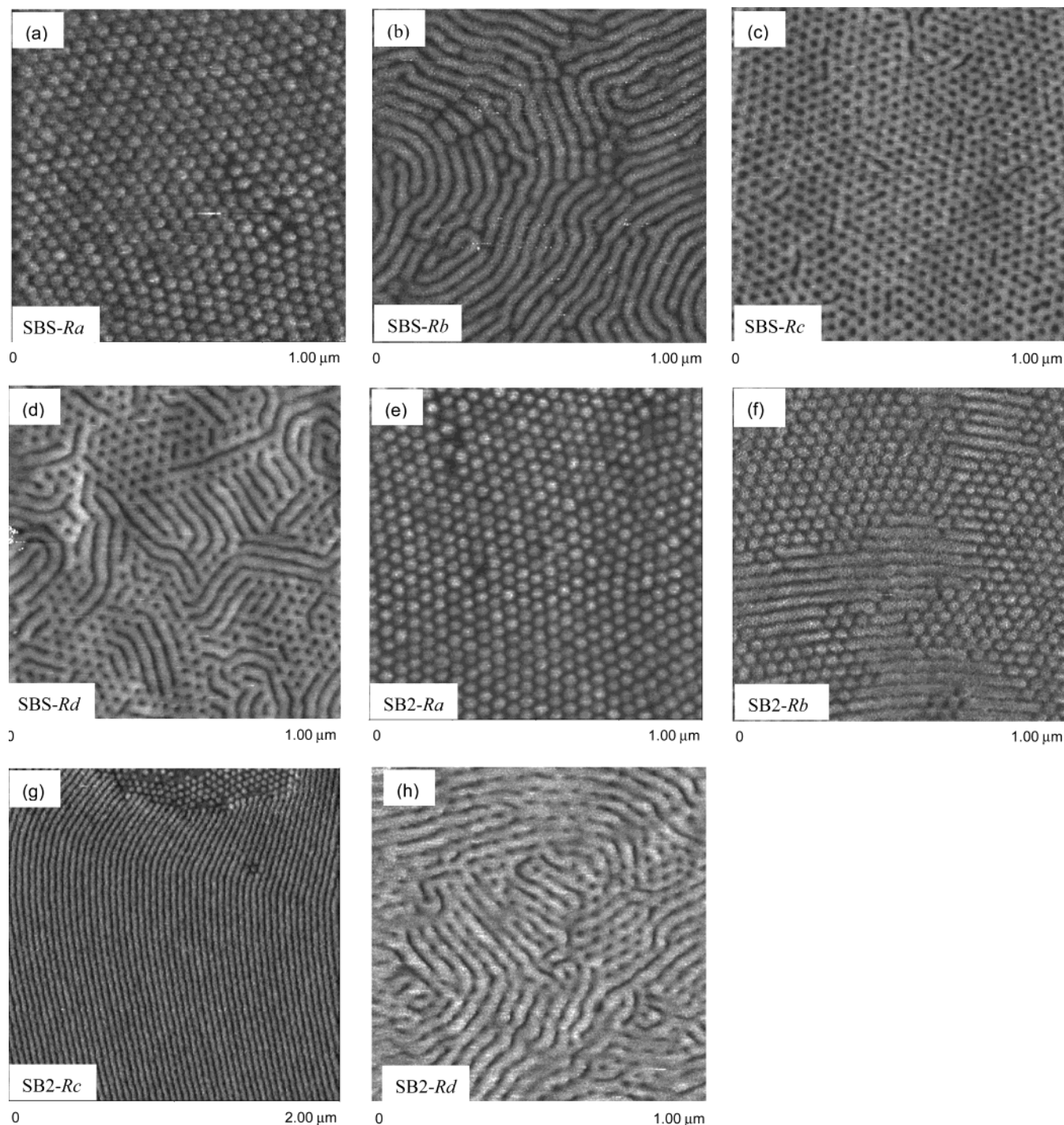
Figure 1. Tapping mode AFM phase images obtained from solution-cast (a)−(d) SBS triblock copolymer films and (e)−(h) SB2 diblock films under different evaporation rates as indicated.

resonant frequency. We operate the microscope at moderate tapping so the glassy PS domains appear dark and the rubbery PB domains appear bright in the images.[29,33]

The same samples were then floated off the mica substrate onto a TEM grid to examine the bulk structure by TEM. The as-cast films have an average thickness of ∼600 nm but tend to be thicker on the edge of the film and thinner in the center. We chose regions that are transmitting to the electron beam (∼150−400 nm) for examination. The JEOL 2010 electron microscope operated at 200 kV accelerating voltage, and the bright-field mode was employed to acquire the TEM images of the samples. To enhance the contrast of the images, the samples were exposed to OsO_4 vapor for ∼30 min, which selectively reacts with the double bond of PB and stays with it. After OsO_4 staining, dark regions of the bright-field TEM

images are identifiable with the PB domains whereas the bright regions are PS.

Results

In this section, we first compare between the microphase morphologies obtained from the SBS triblock and the SB2 diblock cast films at different solvent evaporation rates, *Ra* to *Rd*. Thereafter, the microphase morphologies of the series of SB diblocks (S1 to S4) having similar PS weight fraction but different total molecular weights (from 53.7 to 315.6 kDa) at the two slowest evaporation rates *Rc* and *Rd* will be contrasted to illuminate the effect of molecular weight or χ_{eff} on the phase structure.
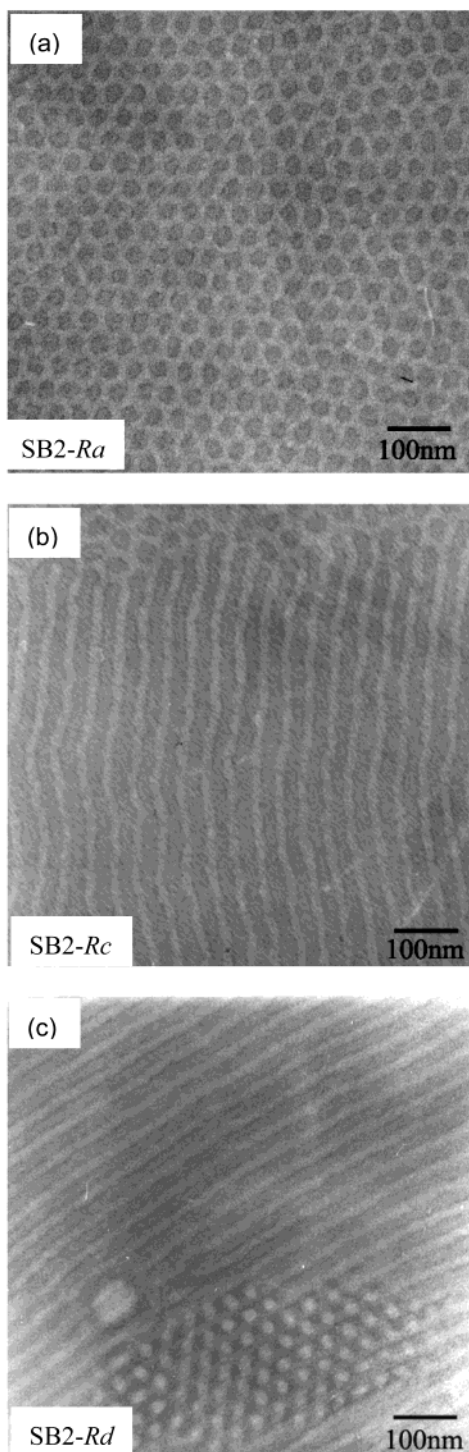
Figure 2. (a–c) Plain-view bright-field TEM micrographs of the same SB2 films shown in parts e, g, and h of Figure 1, respectively. Before imaging, the samples were selectively stained by OsO_4 to enhance the contrast.

Comparison between the SBS Triblock and the SB2 Diblock. It is well established that an ABA triblock will have the same packing characteristics as a stoichiometric diblock if the diblock has the sequence structure $A(^1/_2B)$,[30,34,35] i.e., if the block length of the middle block (B) of an ABA triblock is twice that of the B block of a stoichiometric diblock whereas the block length of each end block (A) of the triblock is the same as that of the diblock. From Table 1, one can see that this condition is approximately fulfilled for SBS and SB2. We thus compare the microstructures of these two

Table 2. Phase Structures of the Block Copolymers as a Function of the Solvent Evaporation Rate[a]
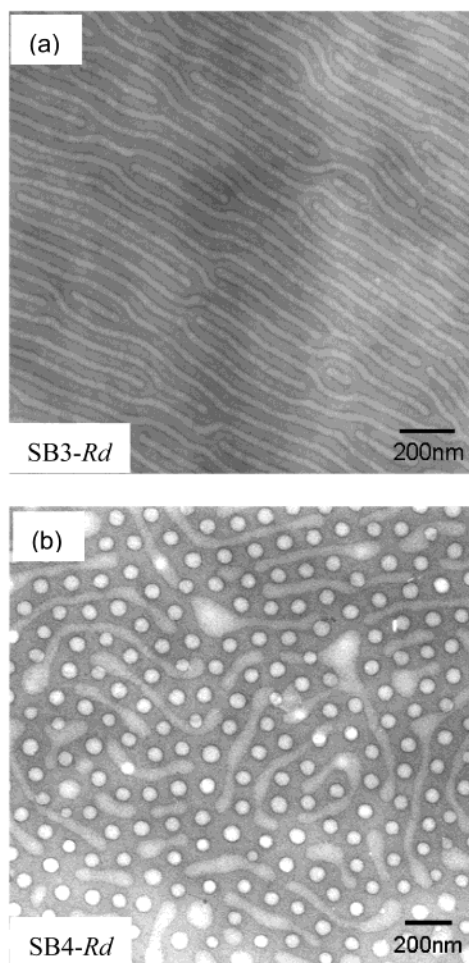
	solvent evaporation rate, R			
	Ra	*Rb*	*Rc*	*Rd*
SBS	IS	IC	NC	NC
SB1	IC	IC	IC and NC	NC
SB2	IS	IS and IC	IC	NC
SB3	NC	NC	NC	NC
SB4	NC	NC	NC	NC

[a] IS = inverted sphere, IC = inverted cylinder, NC = normal cylinder.
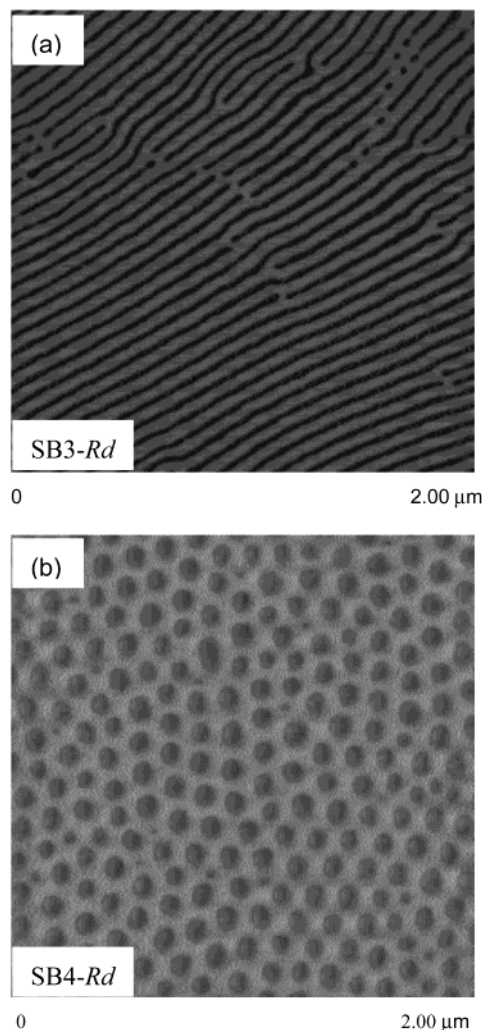
Figure 3. Tapping mode AFM phase images obtained from thin films of (a) SB3 and (b) SB4 obtained at the slowest evaporation rate, *Rd*.

samples for the effect of different sequence structure on the phase separation behavior. The TM-AFM phase-contrast images of thin films of SBS and SB2 from different evaporation rates are shown in Figure 1. With the SBS films, the microstructure (Figure 1a–d) changes from inverted spheres (i.e., PB spheres or cylinders in a PS matrix) to definitely inverted PB cylinders and finally to normal cylinders (i.e., PS cylinders in a PB matrix) as the solvent evaporation rate decreased from *Ra* to *Rd*. This is consistent with the result we obtained before.[29] Figure 1e–h displays the TM-AFM images of the SB2 films. It is apparent that both SBS and SB2 exhibit qualitatively the same inverted-to-normal phase transition behaviors. To better corroborate the 3-dimensional microstructures of these samples, we reexamined

Figure 4. Plain-view bright-field TEM micrographs of thin films of (a) SB3 and (b) SB4 obtained at the slowest evaporation rate, *Rd*.

the same SBS and SB2 films with BF-TEM. Since the thickness of the films studied is 150−400 nm and the domain size of SBS and SB2 is ∼30 nm (Figure 1), TEM plain-view imaging should be able to discern whether the inverted phase seen by TM-AFM is not merely a surface structure but persists down to the bulk. Parts a, b, and c of Figure 2 show the TEM images obtained from the same SB2 films displayed in parts e, g, and h of Figure 1, respectively. All phase structures revealed by BF-TEM are consistent with those by TM-AFM shown in Figure 1 and the BF-TEM cross-sectional views of the SBS films reported in our previous study.[29] The transition from vertical PS cylinders to a duplex cylindrical morphology (i.e., simultaneously vertical and in-plane PS cylinders) in the SBS sample evident in Figure 2c,d is consistent with the observation by Libera and Kim.[5,6] These authors proposed that the change in orientation of the morphology was due to the competition between the thermodynamically preferred planar morphology (which has more of the low surface energy PB populating the air surface) and the kinetically preferred vertical morphology, arising from the higher solvent diffusivity in the PB than in the PS microdomains.

Phase Structures of the SB Diblocks of Different Molecular Weights. Comparison between the phase behaviors of various block copolymers examined in this study is summarized in Table 2. A threshold M_w* is apparent between 74 and 102 kDa, above which the

block copolymers always exhibit the normal phase. Below M_w*, formation of the inverted and normal phase can be harnessed by controlling the solvent evaporation rate. We next present the TM-AFM and BF-TEM images of the SB1, SB3, and SB4 samples to justify our assignment of their phase structures in Table 2.

Figures 3 and 4 display the TM-AFM and BF-TEM, respectively, of the SB3 and SB4 films obtained from the slowest evaporation rate, *Rd*. These data clearly uphold the microstructure to be normal cylinders. The normal cylindrical phase was also found among these samples obtained from other evaporation rates, *Ra* to *Rc* (but the data are not shown). For SB1, the phase structure was found to depend on the solvent evaporation rate. Figures 5 and 6 show respectively the TM-AFM and BF-TEM images of SB1 films obtained from different solvent evaporation rates, *Ra* to *Rd*. For the SB1 film obtained at *Rb*, it displays the planar cylindrical morphology (Figures 5a and 6a) for which it is difficult to determine whether the phase structure is inverted or normal. On the basis of the disclination defects illuminated by the white arrows in these figures, we reason that the matrix phase is the minority component (i.e., PS), and hence the sample is in the inverted phase. Similar disclination defects can also be found in the ubiquitous inverted phase structure in Figure 1b, clearly showing the PB cylinders. For the film obtained at a slower evaporation rate of *Rc*, a hybrid structure showing coexistence of the normal and inverted structures was found (Figures 5b1,b2 and 6b). When the solvent evaporation rate was further reduced to *Rd*, the normal phase structure (Figures 5c and 6c) was obtained. It is therefore concluded that the SB1 sample also exhibits the inverted-normal phase transition with variations in the solvent evaporation rate.

Discussion

The similar microstructures found between thin films of SBS and SB2 (Figure 1) demonstrate that the phase behavior of block copolymers has little dependence on the chain architecture (i.e., diblock or triblock). Therefore, the entropic factor proposed earlier[29] could not be the origin for the formation of the inverted phase. On the other hand, Table 2 shows that, among the SB diblock films investigated, only those with molecular weights less than a threshold between 70 and 100 kDa exhibit the inverted phase (under fast evaporation rates). Dominance of the normal phase is expected from enthalpy factors that grow with increasing sample molecular weight. On the contrary, the drive for the formation of the inverted phase is not apparent. To more thoroughly consider the thermodynamics of the problem, we resort to the algebraic expression by Helfand and Wasserman (H−W) to approximate the free energy, *F*, of ABA and AB asymmetric block copolymers that form the hexagonal cylindrical phase.[30] The H−W free energy, at different interaction parameter, α, and degree of polymerization, *N*, was minimized with respect to the cylindrical microstructure period, *D*, assuming the normal and inverted phase, respectively, for both SBS and SB that contain 30 wt % PS. The result for SB diblock, given in a 3-dimensional plot as $\Delta F_{SB}/N_{cell}k_B T$ vs α and *N*, is shown in Figure 7a, where ΔF_{SB} is the difference between the minimum free energy found for the inverted phase of the diblock SB, $F_{SB,inv}$, minus that for the SB normal phase, $F_{SB,norm}$, and N_{cell} is the number of polymers contained in one unit cell of the
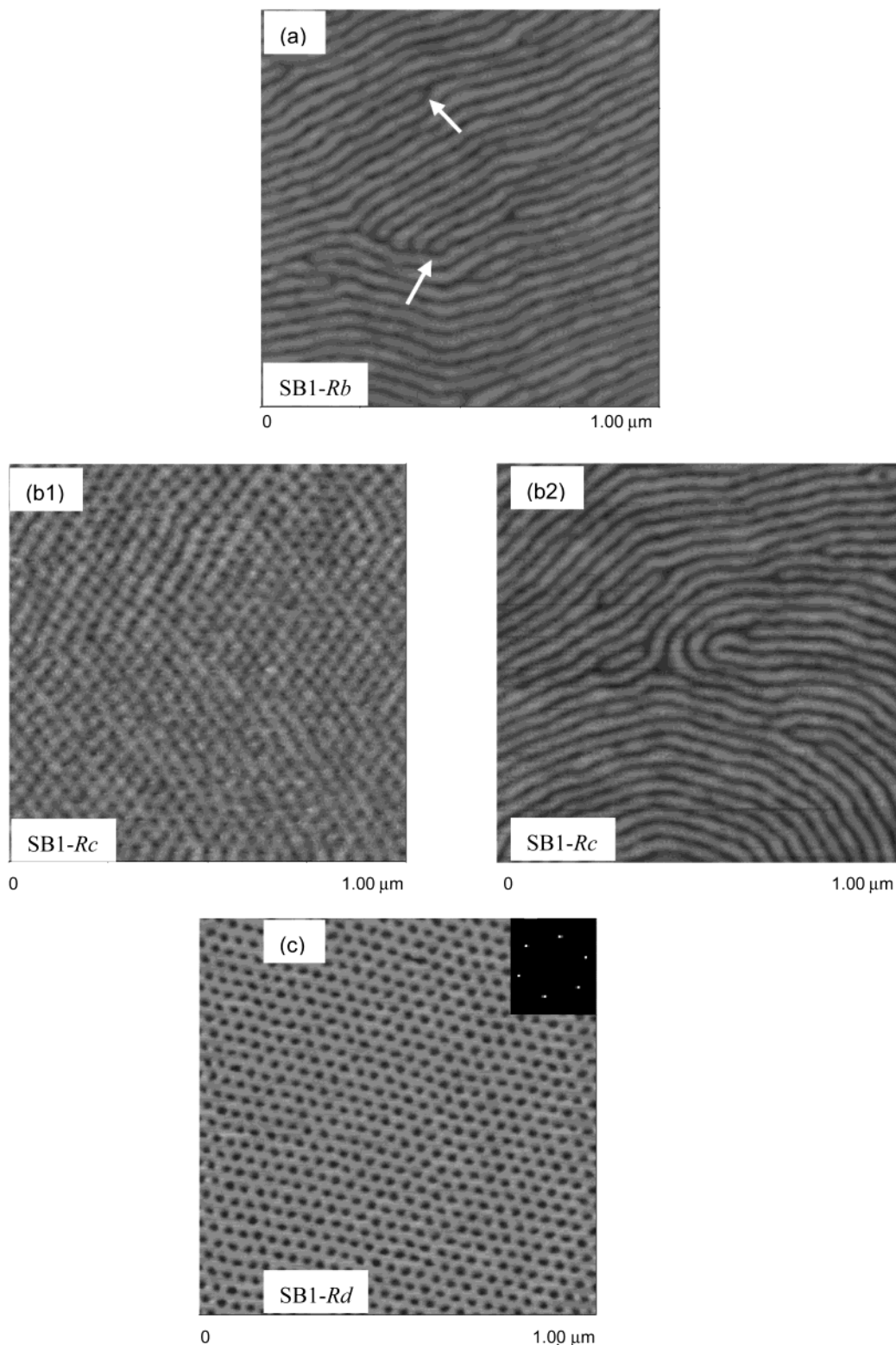
Figure 5. Tapping mode AFM phase images of the SB1 films obtained at different evaporation rates (a) *Rb,* (b1) *Rc* showing the normal phase, (b2) *Rc* showing the inverted phase, and (d) *Rd.*

simple hexagonal structure. The corresponding result obtained for triblock SBS is shown in Figure 7b. Figure 7a,b shows that, for the entire region of $\alpha-N$ phase space that is physically accessible, the free energy of the inverted phase is always higher than that of the normal phase for both SB and SBS. It is interesting to note that $\Delta F_{SBS}/N_{cell}k_BT$ for the triblock is ~8 times larger than $\Delta F_{SB}/N_{cell}k_BT$ for the diblock, which may be qualitatively understood from the balance of different
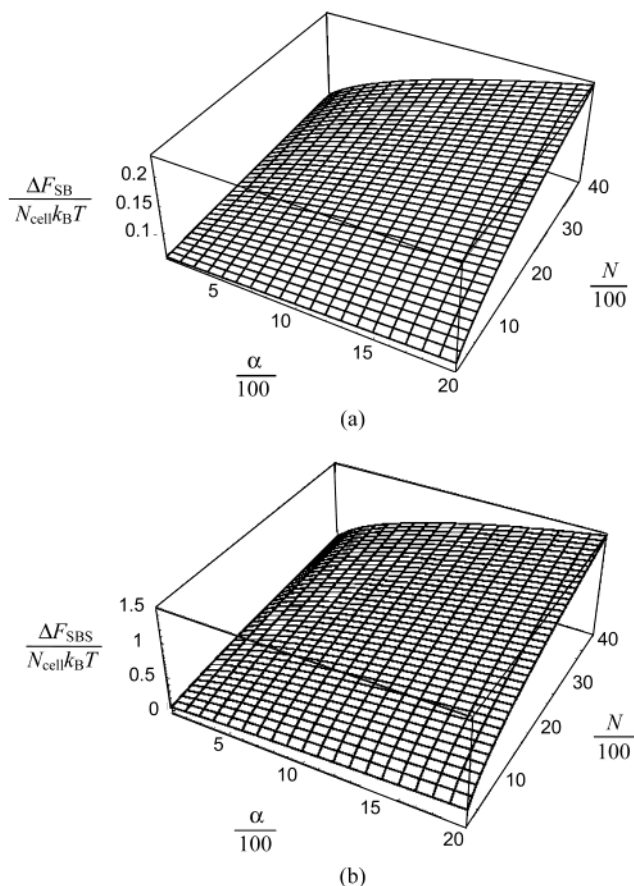
energies in the microstructure.[36] This finding is in accordance with the result listed in Table 2 that the SBS triblock appears to be more resistant to the formation of the inverted phase than the SB diblock. Calculations based on the H−W expression thus show that the inverted phase should not be the equilibrium phase.

The above discussions have considered only the conventional microstructures, namely, lamellae, cylinders, and spheres. More recent experiments have re-
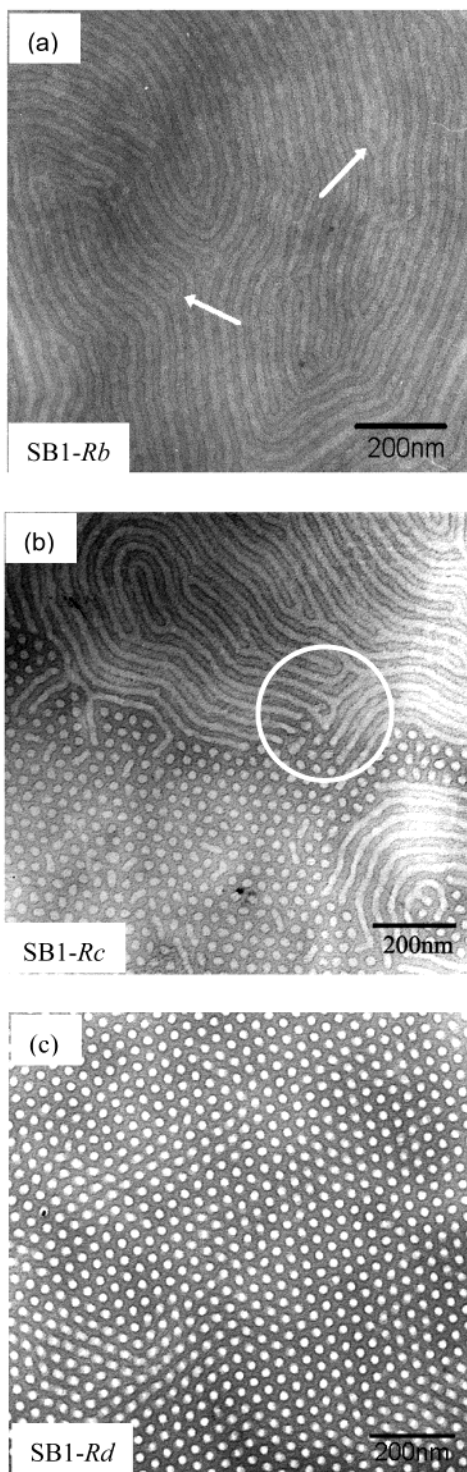
Figure 6. Plain-view bright-field TEM micrographs of the SB1 films obtained at different evaporation rates (*Rb* to *Rd*) as indicated. The white circle in (b) illuminates the boundary between the inverted and normal phase.

Figure 7. Three-dimensional plots of (a) $\Delta F_{SB}/N_{cell}k_B T$ and (b) $\Delta F_{SBS}/N_{cell}k_B T$ as functions of α and N.

vealed more complex microstructures in block copolymers, including the hexagonally modulated layers (HML),[37,38] hexagonally perforated layers (HPL),[37−39] and bicontinuous gyroids (G).[38,40,41] These phases have been found in low molecular weight samples (<∼50 kDa) that are thus more susceptible to fluctuation effects.[37,38] A careful study of Hajduk et al.[38] showed that the HPL and the HML were long-lived nonequilibrium structures, convertible to the G structure upon annealing. Given that the inverted phases were also found in low molecular weight SB and SBS and also have very similar energy as the conventional (normal) phase, it is interesting to consider whether the inverted phase observed here could be related to the "complex" microstructures. Among the three structures mentioned, the HPL are consisting of ABAB stacks, wherein hexagonally packed channels of the majority blocks extend through layers of the minority blocks to form a monocontinuous structure. The structure revealed in Figures 1a,e and 2a of the inverted spherical/cylindrical phase may very well be the bird's-eye view of the perforated layers, which is consistent with a previous note that the surface field in thin films may influence the microstructures and favor formation of the layers parallel to the plane.[41] However, a cross-sectional view of this inverted phase found in our previous study[29] did not show any sign of a layered structure but revealed only PB spheres. Besides, the image shown in Figure 2a has a qualitatively different appearance from the published images of HPL.[42] Therefore, we believe the inverted phase is not related to the HPL structure. Otherwise, the inverted phase could possibly be due to composition fluctuations of the lamellar structure.[37,38]

Probably, the inverted phase is a metastable state formed during the transient when the concentration of the cast film just reaches the semidilute limit (where φ is ∼ 1−2%), and the chains begin to overlap. The unlike blocks retract from each other by mutual repulsions shoving the like blocks into aggregates. Since this happens when the polymer concentration is low, the damping force on the polymer is still small. The polymers may overreact to this transitory force, creating momentary compressions within the aggregates. When

the aggregates stretch out to relax the compressional pressure, the more swift blocks may fill the corona surrounding accretions of the more sluggish block more readily. Since the minor block is more likely swifter because of its shorter length, this process provides a mechanism for the (momentary) formation of the inverted phase. Kinetically speaking, this process will be favored if the free energy of the inverted phase is not much higher than that of the normal phase, and the diffusion rate of the swift block is substantially higher than that of the sluggish block. From Figure 7a,b, $\Delta F_{SB(S)}$ is larger with larger N or larger molecular weight. Furthermore, one also expects the relative diffusion rate between the two blocks to be large if the molecular weight is small enough that the S block is unentangled while the B block is. Both considerations confer reducing favoritism of the formation of inverted phases as the sample molecular weight increases. The apparentness of a threshold M_w^* in Table 2 fits this picture well, and the range of M_w^* observed (70−100 kDa) corresponds to the S-block molecular weight of 20−30 kDa. Although the entanglement molecular weight of PS in the semidilute regime (or more appropriately at the concentration where the said transitory process happens) is not precisely known, the range noted from the experiment is of the order of the entanglement molecular weight of PS in melt, which is not too unreasonable on the basis of the "blob" picture.[43] Given enough time, the inverted phase, if formed, will transform back to the normal phase. In light of the smallness of $\Delta F_{SB(S)}/N_{cell}$ (which is only 1.3% (15%) of the free energy of the normal phase per unit cell), one also expects the domain size of the normal phase recovering from the inverted phase to be large in order to compensate for the interfacial energy between different domains. This is consistent with Figures 5b and 6b revealing the hybrid structure of SB1, which show that the domain size in this transformation is at least 1 μm, comprising ~900 unit cells.

Conclusion

We have examined the formation of inverted phase in a series of solution-cast poly(styrene-*b*-butadiene) (SB) asymmetric diblock copolymers having nearly equal polystyrene (PS) weight fraction of ~30 wt % but different molecular weights, subjected to different evaporation rates. From the similar phase behaviors found between the SBS triblock and the SB2 diblock, we conclude that formation of the inverted phase has little dependence on the block number in the polymer. On the other hand, the phase behavior demonstrates a strong dependence on molecular weight; namely, a threshold molecular weight (or range of molecular weight), between 70 and 100 kDa, was observed above which the inverted phase is never formed. By using the free energy expressions by Helfand and Wasserman, we calculated that the normal phase always has the lower energy than the inverted phase irrespective of the interaction parameter and molecular weight. A mechanism based on kinetic effects was proposed to explain the origin for the formation of inverted phase that has been shown to demonstrate good agreement with experiment.

References and Notes

(1) Sakurai, S.; Momii, T.; Taie, K.; Shibayama, M.; Nomura, S.; Hashimoto, T. *Macromolecules* **1993**, *26*, 485.
(2) Sakurai, S.; Kawada, H.; Hashimoto, T.; Fetters, L. J. *Macromolecules* **1993**, *26*, 5796.
(3) Hajduk, D. A.; Gruner, S. M.; Rangarajan, P.; Register, R. A.; Fetters, L. J.; Honeker, C.; Albalak, R. J.; Thomas. E. L. *Macromolecules* **1994**, *27*, 490.
(4) Sakamoto, N.; Hashimoto, T.; Han, C. D.; Kim, D.; Vaidya, N. Y. *Macromolecules* **1997**, *30*, 5321.
(5) Kim, G.; Libera, M. *Macromolecules* **1998**, *31*, 2569.
(6) Kim, G.; Libera, M. *Macromolecules* **1998**, *31*, 2670.
(7) Hajduk, D. A.; Ho, R. M.; Hillmyer, M. A.; Bates, F. S.; Almdal, K. *J. Phys. Chem. B* **1998**, *102*, 1356.
(8) Ryu, C. Y.; Lodge, P. T. *Macromolecules* **1999**, *32*, 7190.
(9) Kimishima, K.; Koga, T.; Hashimoto, T. *Macromolecules* **2000**, *33*, 968.
(10) Krishnamoorti, R.; Modi, M. A.; Tse, M. F.; Wang, H. C. *Macromolecules* **2000**, *33*, 3810.
(11) Pollard, M.; Russell, T. P.; Ruzette, A. V.; Mayes, A. M.; Gallot, Y. *Macromolecules* **1998**, *31*, 6493.
(12) Ruzette, A.-V. G.; Banerjee, P.; Mayes, A. M.; Pollard, M.; Russell, T. P.; Jerome, R.; Slawecki, T.; Hjelm, R.; Thiyagarajan, P. *Macromolecules* **1998**, *31*, 8509.
(13) Yokoyama, H.; Mates, T. E.; Kramer, E. J. *Macromolecules* **2000**, *33*, 1888.
(14) Li, Z.; Zhao, W.; Liu, Y.; Rafailovich, M. H.; Sokolov, J.; Khougaz, K.; Eisenberg, A.; Lennox, R. B.; Krausch, G. *J. Am. Chem. Soc.* **1996**, *118*, 10892.
(15) Yokoyama, H.; Kramer, E. J.; Rafailovich, M. H.; Sokolov, J.; Schwarz, S. A. *Macromolecules* **1998**, *31*, 8826.
(16) Kim, G.; Han, C. C.; Libera, M.; Jackson, C. L. *Macromolecules* **2001**, *34*, 7336.
(17) Luo, K.; Yang, Y. *Macromolecules* **2002**, *35*, 3722.
(18) Mansky, P.; Tsui, O. K. C.; Russell, T. P.; Gallot, Y. *Macromolecules* **2002**, *32*, 4832.
(19) Leibler, L. *Macromolecules* **1980**, *13*, 1602.
(20) Fredrickson, G. H.; Helfand, E. *J. Chem. Phys.* **1987**, *87*, 697.
(21) Fredrickson, G. H.; Leibler, L. *Macromolecules* **1989**, *22*, 1238.
(22) Olvera de la Cruz, M. *J. Chem. Phys.* **1989**, *90*, 1995.
(23) Hashimoto, T.; Shibayama, M.; Kawai, H. *Macromolecules* **1983**, *16*, 1093.
(24) Shibayama, M.; Hashimoto, T.; Hasegawa, H.; Kawai, H. *Macromolecules* **1983**, *16*, 1427.
(25) Shibayaa, M.; Hashimoto, T.; Kawai, H. *Macromolecules* **1983**, *16*, 1434.
(26) Sakurai, S.; Hashimoto, T.; Fetters, L. J. *Macromolecules* **1996**, *29*, 740.
(27) Lodge, T. P.; Hamersky, M. W.; Hanley, K. J.; Huang, C.-I. *Macromolecules* **1997**, *30*, 6139.
(28) Hanley, K. J.; Lodge, T. P. *J. Polym. Sci., Polym. Phys. Ed.* **1998**, *36*, 3101.
(29) Zhang, Q. L.; Tsui, O. K. C.; Du, B.; Zhang, F. J.; Tang, T.; He, T. B. *Macromolecules* **2000**, *33*, 9561.
(30) Helfand, E.; Wasserman, Z. R. *Macromolecules* **1980**, *13*, 994.
(31) Keller, A.; Pedemonte, E.; Willmouth, F. M. *Polymer* **1970**, *238*, 385.
(32) Aggarwal, S. *Polymer* **1976**, *17*, 938.
(33) Bar, G.; Thomann, Y.; Brandsch, R.; Cantow, H. J. *Langmuir* **1997**, *13*, 3807.
(34) Helfand, E.; Wasserman, Z. R. *Macromolecules* **1976**, *9*, 879.
(35) Helfand, E.; Wasserman, Z. R. *Macromolecules* **1978**, *11*, 960.
(36) The equilibrium free energy is a result of a balance between the interfacial energy between the S and B domains, the conformational entropy loss involved in keeping domain densities uniform, and the loss of entropy involved in localizing the S−B joints in the interphase between domains. It is usually the first and the second terms that dominate, being of the form $2\xi\pi D\gamma/Nk_B T$ (where γ is the interfacial tension, and $\xi = 0.55$ for the normal phase but 0.83 for the inverted phase) and aD^2 (a = constant), respectively. Since N is $\sim D^{1.5}$, the first term tends to increase the domain, period but the second term suppresses it. Furthermore, the difference in the value of a between the normal and inverted phase is larger for the triblock than for the diblock (Figure 2 of ref 30). Therefore, the domain period is larger in the inverted phase than in the normal phase, but the difference is larger in SB than in SBS. (This is confirmed in our calculation of domain period for the two kinds of phases in SB and SBS.) This may

account for the finding of $\Delta F_{SB} > \Delta F_{SBS}$ (Figure 7): The more the domain period of the inverted phase is larger than that of the normal phase, the smaller the free energy rise, $\Delta F_{SB}/N_{cell}$ or $\Delta F_{SBS}/N_{cell}$, will incur in the inverted phase structure from the rise in interfacial energy.

(37) Hamley, I. W.; Koppi, K. A.; Rosedale, J. H.; Bates, F. S.; Almdal, K.; Mortensen, K. *Macromolecules* **1993**, *26*, 5959.

(38) Hajduk, D. A.; Takenouchi, H.; Hillmyer, M. A.; Bates, F. S. *Macromolecules* **1997**, *30*, 3788.

(39) Thomas, E. L.; Anderson, D. M.; Henkee, C. S.; Hoffman, D. *Nature (London)* **1988**, *334*, 598.

(40) Hajduk, D. A.; Harper, P. E.; Gruner, S. M.; Honeker, C. C.; Kim, G.; Thomas, E. L.; Fetters, L. J. *Macromolecules* **1994**, *27*, 4063.

(41) Schulz, M. F.; Bates, F. S.; Almdal, K.; Mortensen, K. *Phys. Rev. Lett.* **1994**, *73*, 86.

(42) See for example: Bailey, T. S.; Pham, H. D.; Bates, F. S. *Macromolecules* **2001**, *34*, 6994, Figure 3b.

(43) de Gennes, P.-G. *Scaling Concepts in Polymer Physics*; Cornell University Press: Ithaca, NY, 1979.